

# Enhancement of the electronic and optical properties of superalkali metal adsorbed $\text{Al}_{10}\text{N}_{10}$ nanocage

Shradha Lakhera <sup>a</sup>, Meenakshi Rana <sup>a,\*</sup>, Vivek Dhuliya <sup>b</sup>

<sup>a</sup> Department of Physics, School of Sciences, Uttarakhand Open University, Haldwani, 263139, Uttarakhand, India

<sup>b</sup> Department of Physics, Gurukul Kangri (Deemed to be University), Haridwar, 249404, Uttarakhand, India

## ARTICLE INFO

### Keywords:

Nanocage  
Superalkali  
Nonlinear optical materials  
Doping  
Intramolecular interactions

## ABSTRACT

The computational designing of the  $\text{Li}_4\text{N}$  and  $\text{Li}_4\text{O}$  as efficient dopants for  $\text{Al}_{10}\text{N}_{10}$  nanocage has been carried out in the present study for the applications of high-performance Nonlinear Optical materials. The density functional theory was employed with UBVP86-6-311G(++,p)def2D2V set of functions for studying the enhanced structural, electronic, and optical properties of  $\text{Al}_{10}\text{N}_{10}$  nanocage after the exohedral substitution of  $\text{Li}_4\text{N}$  and  $\text{Li}_4\text{O}$ . The density of state calculations reveals the formation of a new high energy highest occupied molecular orbital in the combined structure of superalkali and nanocage. This seems to result in a major decrement in the band gap of the complex structure  $\text{Al}_{10}\text{N}_{10}+\text{Li}_4\text{N}$  (0.878eV) and  $\text{Al}_{10}\text{N}_{10}+\text{Li}_4\text{O}$  (0.872eV). The charge transfer from the metal structure towards the nanocage was supported by the natural bond orbital charges. The doping of superalkali gave an intensified value of dipole moment from 1.53 Debye (nanocage) to 10.27 and 14.93 Debye for  $\text{Al}_{10}\text{N}_{10}+\text{Li}_4\text{N}$  and  $\text{Al}_{10}\text{N}_{10}+\text{Li}_4\text{O}$  respectively. This supported the high electronegativities and high intramolecular charge transfer for these complexes. The vibrational spectra reveal the high-intensity modes for stretching the interconnecting bonds between the nanocage and metal structure. The first-order hyperpolarizability for nanocages was remarkably enhanced after superalkali doping. The first-order hyperpolarizability for  $\text{Al}_{10}\text{N}_{10}+\text{Li}_4\text{N}$  and  $\text{Al}_{10}\text{N}_{10}+\text{Li}_4\text{O}$  were computed as  $173.13 \times 10^{-30}$  and  $172.45 \times 10^{-30}$  esu respectively. Thus, the present investigation can be the basis for the experimental fabrication of highly efficient NLO materials and will attract the scientific community to design high-performance NLO materials with exceptional features for widespread applications in optoelectronics.

## 1. Introduction

The past few decades have led to the development of the synthesis and designing of highly efficient Nonlinear Optical (NLO) materials. The rapid development in technology results in designing the desired materials possessing enhanced NLO activity. As the NLO activity is the function of intramolecular interactions, the integration of excess electrons by introducing electron-rich agents is the most effective technique to improve the NLO response of materials [1–3]. Diffused excess electrons give rise to the hyperpolarizability of the materials which is the key factor of NLO response [4]. The study presented by Zhong and the team has introduced a new concept of high NLO activity of materials by introducing moieties with excess electrons via different physical phenomena like adsorption, doping, etc [5,6]. A decrement in the excitation energies was observed for the crucial transitions i.e., the transitions with the highest oscillator strength. This also leads to large

hyperpolarizability and hence a high NLO response [7]. NLO materials with risen hyperpolarizability are employed in different applications like solar conversions, diodes, optoelectronics, optical data storage, dynamic image processing, telecommunications, sensing, optical computing, and many more. Doping has been a trending technique to increase NLO responses. Therefore, many studies have been reported and published in literature where doping has been used to increase the hyperpolarizability of materials. Literature of the prior ab-initio research reports the stability of the  $\text{Al}_n\text{N}_n$ ,  $n = 2-41$  aluminum nitride nanocages [8–11]. Thus, the present study accounts for the rise in the hyperpolarizability of the  $\text{Al}_{10}\text{N}_{10}$  nanocages by doping the superalkalis  $\text{Li}_4\text{N}$  and  $\text{Li}_4\text{O}$ .

The inorganic metal complexes are profoundly employed for NLO applications due to having large values of hyperpolarizability and nonlinear susceptibility due to the availability of excess electrons [12]. These excess electron clouds get collected at the anionic sites which are

\* Corresponding author.

E-mail address: [mrana@uou.ac.in](mailto:mrana@uou.ac.in) (M. Rana).

<https://doi.org/10.1016/j.mssp.2024.108882>

Received 20 May 2024; Received in revised form 2 September 2024; Accepted 3 September 2024

Available online 5 September 2024

1369-8001/© 2024 Elsevier Ltd. All rights are reserved, including those for text and data mining, AI training, and similar technologies.

responsible for high NLO response [13]. In the case of alkali metal doped complexes, a certain decrement in the band gaps was observed and the interaction energies are small. Niu and team stated this fact for the first time during the study of doped alkali metal atoms ( $M = \text{Li, Na, K}$ ) on  $\text{Al}_{12}\text{N}_{12}$  nanocages and observed very small interaction energy between 11.7 and 33.5 kcal/mol and band gap in the range 0.49–0.71 eV [14]. The comparatively smaller size of alkali atoms than the Al and N atoms was found to be the reason behind the low interaction energy. However, the multi-atom alkali dopants were found suitable for the enhancement in the NLO properties [15]. Y. Arshad and the team has employed DFT for exploring the NLO responses of doped  $\text{B}_{12}\text{N}_{12}$  nanocages ( $M@x\text{-B}_{12}\text{N}_{12}$ ; where M is for transition metals including Sc, Ti, V, Cr, Mn, Fe, Co, Ni, Cu, Zn, and  $x = b_{64}, b_{66}, r_6,$  and  $r_4$ ) [16]. A remarkable rise in the hyperpolarizability of  $1.39 \times 10^4$  au was obtained for the  $\text{Sc}@b_{64}\text{-B}_{12}\text{N}_{12}$  complex. A similar kind of work was performed by Khaliq for the investigation of the influence of superalkalis ( $\text{Li}_4\text{N}$  and  $\text{Li}_4\text{O}$ ) doping on the structural, electrical, optical, and NLO responses of the  $\text{Al}_{12}\text{N}_{12}$  nanocage. For the mentioned study, hyperpolarizability of  $5.7 \times 10^4$  au is achieved for the  $\text{Li}_4\text{N}@\text{Al}_{12}\text{N}_{12}$  nanocage [17]. N. Kosar and his team have previously done theoretical research in designing novel inorganic complexes by doping superalkalis ( $\text{Li}_3\text{O}$ ,  $\text{Na}_3\text{O}$ , and  $\text{K}_3\text{O}$ ) on the  $\text{Zn}_{12}\text{O}_{12}$  cluster [18]. The results reveal that doping causes the shifting of excess electrons from superalkalis towards the  $\text{Zn}_{12}\text{O}_{12}$  cluster and enhances the NLO properties of these isomers. Moreover, the designed clusters gave excellent transparency under the ultraviolet region of workable laser conditions. DFT was also employed for analyzing the stability, boundary crossing barriers, and optical (linear and non-linear) properties of  $\text{X}_{12}\text{Y}_{12}$  nano-cages ( $X = \text{B, Al}$  and  $Y = \text{N, P}$ ), and the values of hyperpolarizabilities were found satisfactory enough to validate that the designed nanocages respond tremendously to the NLO properties [19]. A. rad and K. Ayub did a comparative study using DFT to study the chemical adsorption of guanine on  $\text{Al}_{12}\text{N}_{12}$ ,  $\text{Al}_{12}\text{P}_{12}$ ,  $\text{B}_{12}\text{N}_{12}$ , and  $\text{B}_{12}\text{P}_{12}$  nano-cages [20]. Literature has accounted for numerous research articles with a wide variety of designed nanocages and developed their purpose in the field of NLO materials.

The incorporation of alkali metal atoms on nanocages is the proven way to design the potential high NLO responsive materials with high hyperpolarizabilities. However, for the first time, the work has been performed for  $\text{Al}_{10}\text{N}_{10}$  nanocage with doped superalkalis. The DFT tools were used to check the stability of the designed nanocage. This theoretical study intends to design and investigate the  $\text{Al}_{10}\text{N}_{10}+\text{Li}_4\text{N}$  and  $\text{Al}_{10}\text{N}_{10}+\text{Li}_4\text{O}$  complexes. The specific objective of this work is to explore the NLO responses of the mentioned complexes for their leading application in various advanced fields like optoelectronics and photonics. The present research work will provide new insights into the designing of new NLO active structures after the introduction of superalkalis. The reported study will serve as a base for future experimental studies on NLO materials.

## 2. Computational procedure and calculation

The geometries of probe  $\text{Al}_{10}\text{N}_{10}$ ,  $\text{Al}_{10}\text{N}_{10}+\text{Li}_4\text{N}$ , and  $\text{Al}_{10}\text{N}_{10}+\text{Li}_4\text{O}$  complex were optimized to the ground state using BVP86/6-311G(+++d, p) set of functions of density functional theory (DFT) (Fig. 1). In the literature, it was noticed that the calculations done with the alkali metals were more perfect in the case of the aforementioned basis set of functions [21]. Thus, these functionals were found more accurate in the case of title complexes. The ground state geometry optimization was followed by the frequency calculations for optimized complexes as true maxima using the same set of functions. The interaction of the nanocage  $\text{Al}_{10}\text{N}_{10}$  and superalkali ( $\text{Li}_4\text{N}$  and  $\text{Li}_4\text{O}$ ) was equated using equation (1):

$$E_{\text{interaction}} = E_{(E_{\text{Al}_{10}\text{N}_{10}} + \text{super-alkali})} - (E_{\text{Al}_{10}\text{N}_{10}} + E_{\text{superalkali}}) \quad (1)$$

The band gap was computed for  $\text{Al}_{10}\text{N}_{10}+\text{Li}_4\text{N}$  and  $\text{Al}_{10}\text{N}_{10}+\text{Li}_4\text{O}$  complex using the energies of the highest occupied ( $E_{\text{HOMO}}$ ) and lowest unoccupied ( $E_{\text{LUMO}}$ ) molecular orbitals using equation (2):

$$\Delta E = E_{\text{LUMO}} - E_{\text{HOMO}} \quad (2)$$

The chemical reactivity of the title complexes was studied by computing the global reactivity parameters using the set of Koopman's

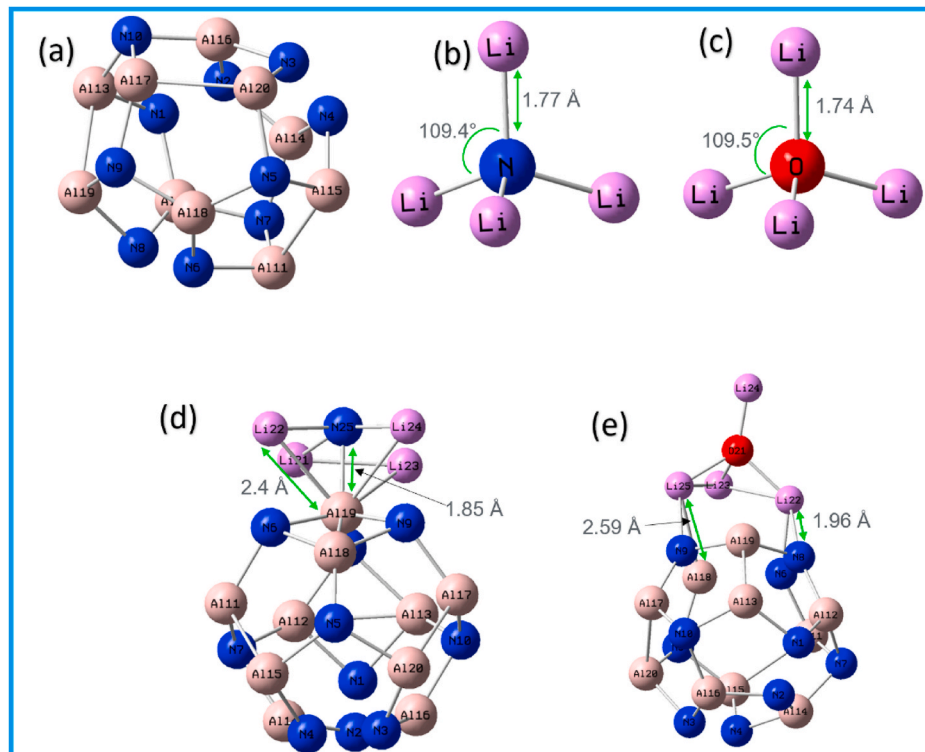


Fig. 1. Optimized structure of (a)  $\text{Al}_{10}\text{N}_{10}$ , (b)  $\text{Li}_4\text{N}$ , (c)  $\text{Li}_4\text{O}$ , (d)  $\text{Al}_{10}\text{N}_{10}+\text{Li}_4\text{N}$ , and (e)  $\text{Al}_{10}\text{N}_{10}+\text{Li}_4\text{O}$  using UBVP86-6-311G (+++d,p) def2D2V set of functions.

equation mentioned in the previous studies [22,23].

The second-order perturbation Fock–matrix was computed using natural bond orbital analysis for monitoring the donor-acceptor interactions in the title nanocages. Stabilization energy ( $E(2)$ ) corresponding to each donor (i) and acceptor (j) atom was computed using equation (3):

$$E(2) = \Delta E_{ij} - q_i \left( \frac{f_{ij}^2}{E_j - E_i} \right) \quad (3)$$

Where  $F(i,j)$  -Fock matrix element between i and j NBO orbitals,  $E_j$  and  $E_i$  are the energies of the acceptor and donor NBOs. The density of states (DOS) analysis was done to account for the average space of the various states occupied by the system. The DOS spectra was obtained employing the Gauss Sum software [24].

The optimized geometries were used for the vibrational and electronic properties of the title nanocages. The optimized geometries and spectral calculations were done using Gaussian 09 packages and analyzed using the Gauss View program [25,26]. The Raman intensity of the higher frequency vibrational modes were calculated using the equation:

$$I = \frac{f(\nu_o - \nu_i)^4 S_i}{\nu_i \left[ 1 - \exp\left(-\frac{h\nu_i}{kT}\right) \right]} \quad (4)$$

where  $I$  is Raman intensity of the vibrational mode,  $f$  is a constant with value  $10^{-12}$ ,  $\nu_o$  has a value  $9398.5 \text{ cm}^{-1}$ .  $\nu_i$  and  $S_i$  is the vibrational wavenumber and Raman activity of the selected mode respectively.  $h$  is Planck constant with  $e 4.1357 \times 10^{-15} \text{ eV K}^{-1}$ ,  $c$  is the speed of light having value  $3 \times 10^8 \text{ m/s}$ ,  $K$  is Boltzmann constant with value  $8.6173 \times 10^{-5} \text{ eV K}^{-1}$ , and  $T$  is temperature  $293.5 \text{ K}$ . The electronic spectra were simulated for the nanocages by employing time-dependent DFT (TD-DFT) and performing energy optimization using same set of functions.

The application of the title complexes for  $\text{Al}_{10}\text{N}_{10}+\text{Li}_4\text{N}$  and  $\text{Al}_{10}\text{N}_{10}+\text{Li}_4\text{O}$  as efficient NLO materials was defined by computing the polarizability parameters. The value of dipole moment ( $\mu_{total}$ ) was computed using tensor components as equation (5) [27,28]:

$$\mu_{total} = \left( \mu_x^2 + \mu_y^2 + \mu_z^2 \right)^{\frac{1}{2}} \quad (5)$$

The polarizability ( $\alpha_{total}$ ) is the measure of the optical linearity of the complex and first-order hyperpolarizability ( $\beta_{total}$ ) is the parameter that defines the optical nonlinearity. These parameters were calculated using equations (6) and (7) by the finite field theory approach [27,28]:

$$\alpha_{total} = \frac{1}{2} (\alpha_{xx} + \alpha_{yy} + \alpha_{zz}) \quad (6)$$

$$\beta_{total} = \left[ (\beta_{xxx} + \beta_{yyy} + \beta_{zzz})^2 + (\beta_{yyy} + \beta_{zzz} + \beta_{xxx})^2 + (\beta_{zzz} + \beta_{xxx} + \beta_{yyy})^2 \right]^{\frac{1}{2}} \quad (7)$$

where  $\beta_{xxx}$ ,  $\beta_{yyy}$ , and  $\beta_{zzz}$  are the tensor components of hyperpolarizability.

### 3. Results and discussion

#### 3.1. Structure and charge analysis

The geometry of  $\text{Al}_{10}\text{N}_{10}$  was drawn with a closed structure of eight pentagons made with ten Al atoms and ten Nitrogen atoms. The geometry was optimized to the ground level. The optimized geometries of the nanocage, dopants, and complexes are illustrated in Fig. 1. The optimized bonds Al – N have a bond length of  $1.8 \text{ \AA}$ , Al – Al bonds have bond lengths of  $2.5 \text{ \AA}$ , and N – N have bond length around  $1.5 \text{ \AA}$ . The optimized geometry of the  $\text{Al}_{10}\text{N}_{10}$  nanocage is illustrated in Fig. 1 (a). Lithium atom was found the most efficient dopant for increasing the

polarizability of the clusters. Nitrogen atom and oxygen atom act as strong electron donating and electron withdrawing atoms Thus,  $\text{Li}_4\text{N}$  and  $\text{Li}_4\text{O}$  (Fig. 1(b) and (c)) were taken as the dopants exohedrally. The optimized geometries of  $\text{Al}_{10}\text{N}_{10}+\text{Li}_4\text{N}$  and  $\text{Al}_{10}\text{N}_{10}+\text{Li}_4\text{O}$  complexes were illustrated in Fig. 1(d) and (e). Both the structures were optimized with the same set of functions as taken for the nanocage and the geometries of  $\text{Li}_4\text{N}$  and  $\text{Li}_4\text{O}$  were optimized at the bond length of  $1.77 \text{ \AA}$  and  $1.74 \text{ \AA}$  respectively for N – Li and O – Li bonds. The dipole moment of the  $\text{Al}_{10}\text{N}_{10}$  nanocage was seen to rise from  $1.538$  Debye to  $10.279$  Debye for  $\text{Al}_{10}\text{N}_{10}+\text{Li}_4\text{N}$  and  $14.932$  Debye for  $\text{Al}_{10}\text{N}_{10}+\text{Li}_4\text{O}$ . This might be due to the enhanced molecular interactions between the nanocage and the dopants. The interaction energies for the  $\text{Al}_{10}\text{N}_{10}+\text{Li}_4\text{N}$  and  $\text{Al}_{10}\text{N}_{10}+\text{Li}_4\text{O}$  complexes were computed as  $17562.1 \text{ kcal/mol}$  and  $1837.16 \text{ kcal/mol}$  respectively. The significant difference between the interaction energies was observed due to the variation in the ground state optimized energies of the superalkalis. The higher value of interaction energy for  $\text{Al}_{10}\text{N}_{10}+\text{Li}_4\text{N}$  complex as compared to  $\text{Al}_{10}\text{N}_{10}+\text{Li}_4\text{O}$  complex reveals immense high intramolecular interactions in  $\text{Al}_{10}\text{N}_{10}+\text{Li}_4\text{N}$  than  $\text{Al}_{10}\text{N}_{10}+\text{Li}_4\text{O}$ .  $C1$  point group symmetry was observed for both complexes. In  $\text{Al}_{10}\text{N}_{10}+\text{Li}_4\text{N}$ , the nitrogen atom of the dopant was observed to interact with the  $19\text{Al}$  atom of the nanocage. Along with the N atom, the Li atoms also participated in the intramolecular interactions with the nanocage with bond length of  $1.85 \text{ \AA}$  for Li – Al bond. But in the case of  $\text{Al}_{10}\text{N}_{10}+\text{Li}_4\text{O}$ , no such interaction between the  $21\text{O}$  atom of the dopant and Al atoms was noticed. The  $22\text{Li}$  and  $25\text{Li}$  atoms of the dopant interacts with the  $8\text{N}$ ,  $9\text{N}$ ,  $6\text{N}$  and  $18\text{Al}$  atoms with Li – Al bond of length  $2.59 \text{ \AA}$  and Li – N bond length of  $1.96 \text{ \AA}$ . The adsorption energy of  $-80.43 \text{ eV}$  and  $-0.40 \text{ eV}$  were observed for the  $\text{Al}_{10}\text{N}_{10}+\text{Li}_4\text{N}$  and  $\text{Al}_{10}\text{N}_{10}+\text{Li}_4\text{O}$  complexes respectively.

#### 3.2. Molecular electrostatic potential and counterplots analysis

The MEP surfaces were plotted to identify the nucleophilic and electrophilic regions of the nanocages. The red and yellow color of the MEP surface is settled over the electron-withdrawing atoms whereas the blue regions are over the electron-donating atoms [29]. The N atoms of the nanocage acted as electron-donating and the Al atoms acted as electron-withdrawing agents. Due to the equal counts of N and Al atoms in the  $\text{Al}_{10}\text{N}_{10}$  nanocage, the MEP surface of the nanocage was obtained full of blue and red regions (Fig. 2 (a)). The counter plots of  $\text{Al}_{10}\text{N}_{10}$  nanocage (Fig. 2 (b)) were also found uniformly distributed over the geometry of the nanocage showing the balanced effect of the field on the nanocage. The MEP surfaces plotted for the nanocage after the substitution of the superalkali however, neglect the effect of Al and N atoms and reveal the enhanced involvement of the superalkali in the intramolecular charge transfer (ICT). The major portion of the  $\text{Li}_4\text{N}$  in its MEP surface (Fig. 2 (c)) acts as electron-donating parts. This might be due to the donating nature of the lithium atoms. The MEP of  $\text{Al}_{10}\text{N}_{10}+\text{Li}_4\text{N}$  (Fig. 2(d)) shows the transfer of the charge cloud from superalkali toward the nanocage. The counterplots of the  $\text{Al}_{10}\text{N}_{10}+\text{Li}_4\text{N}$  (Fig. 2 (e)) also support the transfer of the charge cloud from superalkali towards the nanocage. A similar kind of nature was not observable in the case of  $\text{Al}_{10}\text{N}_{10}+\text{Li}_4\text{O}$ . Electron-donating nature of the superalkali  $\text{Li}_4\text{O}$  (Fig. 2 (f)) was observed individually but after the formation of the complex nanocage  $\text{Al}_{10}\text{N}_{10}+\text{Li}_4\text{O}$  (Fig. 2 (g)), the nanocage became chemically neutral. This might be due to the negligible charge variation between the nanocage and the superalkali. The counterplot of  $\text{Al}_{10}\text{N}_{10}+\text{Li}_4\text{O}$  (Fig. 2 (h)) have verified the role of ICT in both the superalkali-doped nanocages. It can also be said that the  $\text{Li}_4\text{O}$  is not interacting with the nanocage as  $\text{Li}_4\text{N}$  is interacting. This can be supported by the optimized geometries of the nanocages shown in Fig. 1(d) and (e). Fig. 1(d) shows the complete bond formation of the atoms of  $\text{Li}_4\text{N}$  with the nanocage, but in the case of  $\text{Li}_4\text{O}$ , complete superalkali did not form a bond with the nanocage completely. This supports the outcomes predicted by MEP surfaces that there is the availability of ICT in the  $\text{Al}_{10}\text{N}_{10}+\text{Li}_4\text{N}$  complex but any intramolecular interactions are missing in the  $\text{Al}_{10}\text{N}_{10}+\text{Li}_4\text{O}$  complex. In

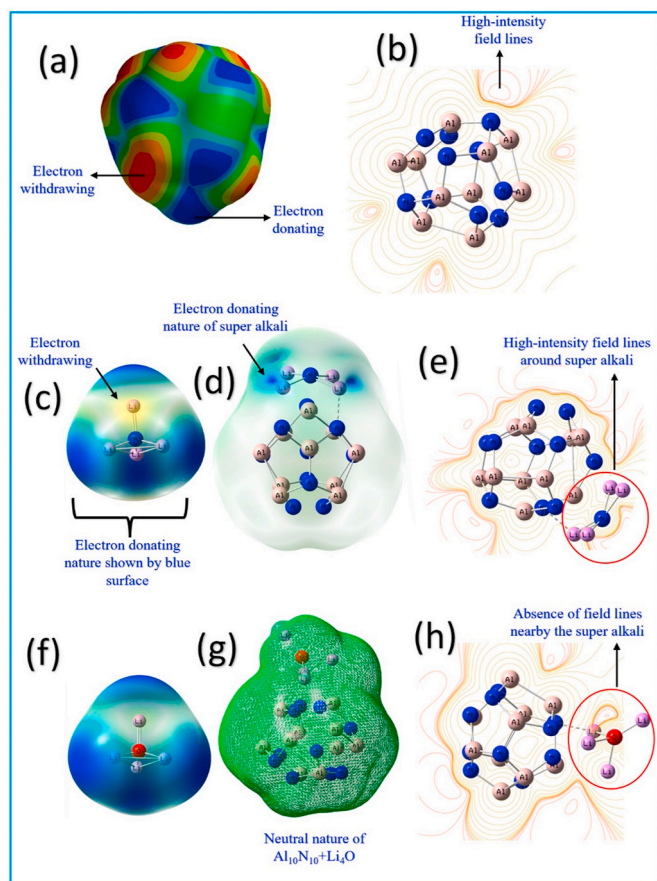


Fig. 2. Molecular electrostatic potential surface of (a)  $\text{Al}_{10}\text{N}_{10}$ , (b)  $\text{Li}_4\text{N}$ , (c)  $\text{Al}_{10}\text{N}_{10}+\text{Li}_4\text{N}$  (d)  $\text{Li}_4\text{O}$ , and (e)  $\text{Al}_{10}\text{N}_{10}+\text{Li}_4\text{O}$  and counterplots of (f)  $\text{Al}_{10}\text{N}_{10}$ , (g)  $\text{Li}_4\text{N}$ , and (h)  $\text{Li}_4\text{O}$ .

the case of  $\text{Al}_{10}\text{N}_{10}+\text{Li}_4\text{N}$ , it is observed that the complex is uniformly surrounded by the counterplots. But in the case of  $\text{Al}_{10}\text{N}_{10}+\text{Li}_4\text{O}$ , there were no counterplots observed around the superalkali. This shows that the field lines immensely affect the  $\text{Li}_4\text{N}$  but there is no such effect of field lines experienced by the  $\text{Li}_4\text{O}$  superalkali. Thus, the settling of the counterplots was in good agreement with the MEP surfaces.

### 3.3. Chemical reactivity analysis

The chemical reactivity of the probe nanocage and the complexes was estimated by computing the chemical reactivity descriptors like ionization potential (IP), electron affinity (EA), chemical potential (CP), electronegativity ( $\chi$ ), chemical hardness ( $\eta$ ), and softness (S). The electrophilicity index ( $\omega$ ) was calculated to predict the donating or accepting character of the nanocage and the dopants respectively. The values of the FMO parameters have been listed in SD 1 and the comparison of the FMP parameters is illustrated in Fig. 3. The band gap for the probe nanocage was computed as 5.98 eV by subtracting the energies of the highest occupied and lowest unoccupied molecular orbitals. The band gap was lower for the dopants  $\text{Li}_4\text{N}$  (4.788 eV) and  $\text{Li}_4\text{O}$  (2.01 eV). This seems to result in a major decrement in the band gap of the complex structure  $\text{Al}_{10}\text{N}_{10}+\text{Li}_4\text{N}$  (0.878eV) and  $\text{Al}_{10}\text{N}_{10}+\text{Li}_4\text{O}$  (0.872eV). IP was reduced and EA was increased after the introduction of the dopant. This shows the enhanced activity of the complex in attracting the charge cloud for intramolecular interactions. The value of  $\omega$  was also enhanced after the adsorption of the dopant showing the availability of the accepting and donating power of the complexes. The value of electron-donating power for the probe nanocage was higher than that of the dopant. After the formation of the complex. A higher value of the

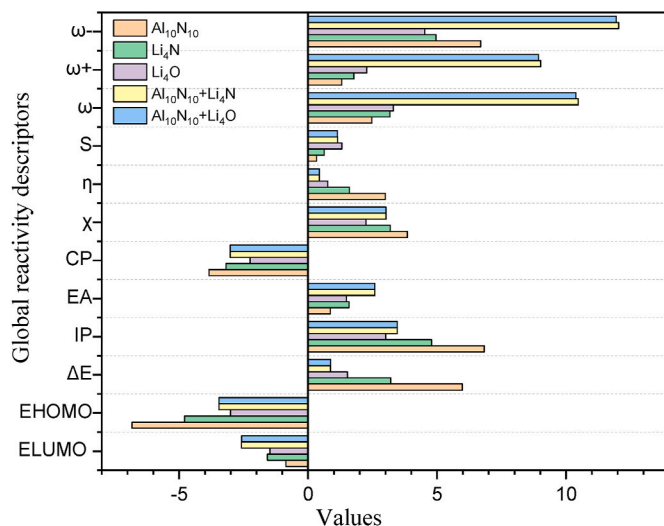
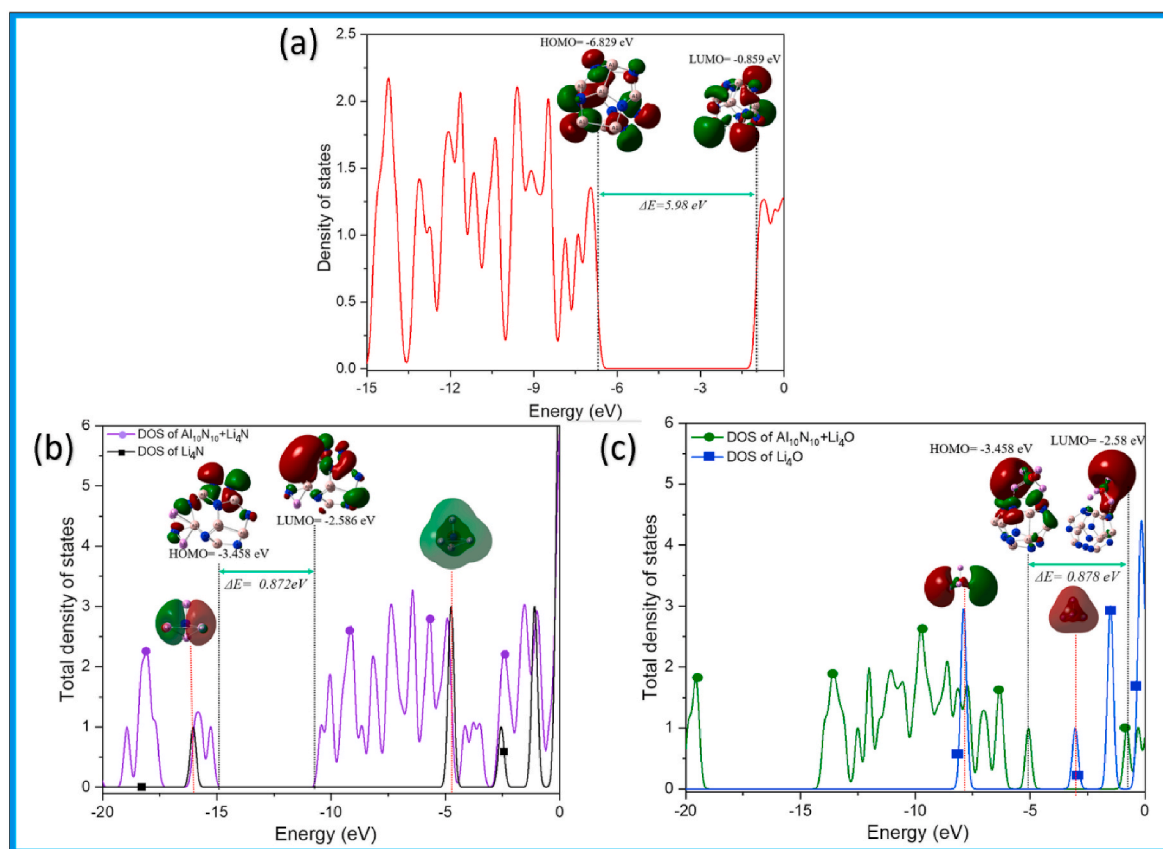


Fig. 3. Comparison of the values of global reactivity descriptors for  $\text{Al}_{10}\text{N}_{10}$ ,  $\text{Li}_4\text{N}$ ,  $\text{Li}_4\text{O}$ ,  $\text{Al}_{10}\text{N}_{10}+\text{Li}_4\text{N}$ , and  $\text{Al}_{10}\text{N}_{10}+\text{Li}_4\text{O}$ .

electron-accepting power was obtained for the dopants. Thus, the values of the electrophilicity index show the charge transfer from the nanocage toward the  $\text{Li}_4\text{N}$  and  $\text{Li}_4\text{O}$  dopants. The global reactivity descriptors analysis reveals the high reactivity of the complexes.

### 3.4. Density of states and orbitals analysis

Fig. 4 illustrates the density of states for  $\text{Al}_{10}\text{N}_{10}$  (Fig. 4 (a)),  $\text{Al}_{10}\text{N}_{10}+\text{Li}_4\text{N}$  (Fig. 4 (b)), and  $\text{Al}_{10}\text{N}_{10}+\text{Li}_4\text{O}$  (Fig. 4 (c)). For a better understanding, the HOMO-LUMO surfaces have been illustrated in the DOS spectra of the respective complexes. The positive areas or the moieties with excessive electrons available for donation are represented by green color and the negative charge or the electron-withdrawing nature is represented by the red-colored surface [30]. The HOMO-LUMO surfaces in the probe  $\text{Al}_{10}\text{N}_{10}$  nanocage were distributed throughout the geometry of the nanocage. The band gap, however, was found to be higher for the probe nanocage. The firm distribution of the orbital surfaces over the probe  $\text{Al}_{10}\text{N}_{10}$  indicates the stable nature of the nanocage and participation of N as well as Al atoms in maintaining the chemical reactivity. The main point of observation was the significant decrement in the band gap of the nanocage after the adsorption of superalkalis. The energies of HOMO-LUMO were significantly changed for nanocage and superalkali complex when compared to that of probe nanocage. The shifting of the HOMO and LUMO energy levels results in the reduction of the band gap of the complexes. The band gap of the probe nanocage decreased to 0.872 eV and 0.878 eV for  $\text{Al}_{10}\text{N}_{10}+\text{Li}_4\text{N}$ , and  $\text{Al}_{10}\text{N}_{10}+\text{Li}_4\text{O}$  respectively. Thus, the superalkali introduced as adsorbate in the present study was found efficient in decreasing the band gap of the nanocage. The HOMO-LUMO surfaces of the superalkali adsorbed nanocages  $\text{Al}_{10}\text{N}_{10}+\text{Li}_4\text{N}$ , and  $\text{Al}_{10}\text{N}_{10}+\text{Li}_4\text{O}$  show the shifting of the negative surface over the superalkali in LUMO. This shifting of orbitals can be interpreted as the formation of new HOMO levels in superalkali-doped  $\text{Al}_{10}\text{N}_{10}$  complexes. In other words, the introduced superalkalis can be interpreted as the dominant contributors in the formation of the new HOMO levels. The red orbital surfaces were seen to dislocate from the nanocage over the adsorbed superalkali. This dislocation reveals that the superalkalis acts as electron-withdrawing agents and the nanocage as the donating atom. Additionally, the DOS spectrum of superalkalis  $\text{Li}_4\text{N}$  and  $\text{Li}_4\text{O}$  were singularly shown in Fig. 4(b) and (c) respectively. Higher peaks of the density of states were observed near the LUMO. Moreover, the HOMO-LUMO surfaces seem to get shifted for superalkali but the  $\text{Li}_4\text{N}$  singularly acts as the donor and  $\text{Li}_4\text{O}$  singularly acts as the acceptor parts. In the adsorbed state, the nanocage complex



**Fig. 4.** HOMO and LUMO with respective energies and DOS spectra of (a)  $\text{Al}_{10}\text{N}_{10}$ , (b)  $\text{Al}_{10}\text{N}_{10}+\text{Li}_4\text{N}$ , and (c)  $\text{Al}_{10}\text{N}_{10}+\text{Li}_4\text{O}$  using illustrating the reduced band gap after the adsorption of superalkali structures.

was observed to exhibit intramolecular interactions. The availability of the orbitals in LUMO of complexes reveals the transfer of the charge cloud density from the nanocage towards the superalkalis. Thus, the DOS analysis reveals the possibility of the occurrence of the ICT from the nanocage to the superalkali.

### 3.5. Natural bond orbital and charge analysis

The inter and intramolecular interactions were predicted using the NBO analysis. In the present paper, the NBO analysis is employed to identify the major and contributory bonds in ICT. The delocalization of the charge cloud from donor NBO towards acceptor NBO leads to the occurrence of high conjugation within the molecule that enhances the stability of the nanocage [31]. The measure of the stability of the donor and acceptor NBOs is therefore described by the stabilization energy that is evaluated using equation (4). The calculated stabilization energy has been listed in Table 1. The probe nanocage  $\text{Al}_{10}\text{N}_{10}$  gave high stabilization energy for the interactions between 4N–15Al and 6N–11Al bonds. Most of the interactions having high stabilization energy were due to the interaction between N – Al bonds. The equal count of Al and N atoms results in the stabilized geometry of the probe nanocage. Moreover, the Mulliken and natural charge distribution reveals the negative contribution of N atoms and the positive contribution of Al atoms. The Mulliken and natural charge distribution of the nanocages has been listed in SD 2. In the case of  $\text{Al}_{10}\text{N}_{10}+\text{Li}_4\text{N}$ , the structural analysis and MEP surface analysis revealed an equal interaction between the 19Al and Li atoms. A similar kind of equal stabilization was obtained by NLO analysis. The bonds between the 19Al and Li atoms of the superalkali were stabilized with nearly equal stabilization energy. Moreover, the value of stabilization energy was found higher for these bonds. This reveals the active participation of the superalkali in stable complex formation via

**Table 1**  
Second Order Perturbation Theory Analysis of Fock Matrix in NBO Basis for  $\text{Al}_{10}\text{N}_{10}$ ,  $\text{Al}_{10}\text{N}_{10}+\text{Li}_4\text{N}$ , and  $\text{Al}_{10}\text{N}_{10}+\text{Li}_4\text{O}$  nanocage.

S. no.	Donor NBO (i)	Acceptor NBO (j)	$E(2)$ (kcal/mol)	$E(j)-E(i)$ (au)	$F(i,j)$ (au)
<b><math>\text{Al}_{10}\text{N}_{10}</math></b>					
1.	BD (1N-12Al)	BD* (2N-13Al)	17.24	0.76	0.103
2.	BD (3N-16Al)	BD* (2N-20Al)	41.53	0.60	0.141
3.	BD (4N-15Al)	BD* (6N-11Al)	116.52	0.01	0.103
4.	BD (5N-20Al)	BD* (9N-17Al)	86.96	0.02	0.091
5.	BD (6N-11Al)	BD* (11Al – 15Al)	30.96	0.02	0.079
6.	BD* (7N-12Al)	BD* (1N-12Al)	43.63	0.03	0.105
7.	BD* (2N-17Al)	BD* (2N-16Al)	45.18	0.03	0.076
<b><math>\text{Al}_{10}\text{N}_{10}+\text{Li}_4\text{N}</math></b>					
1.	BD (19Al-25N)	LP* (21Li)	5.91	0.98	0.097
2.	BD (19Al-25N)	LP* (22Li)	6.68	1.14	0.111
3.	BD (19Al-25N)	LP* (23Li)	5.82	1.26	0.109
4.	BD (19Al-25N)	LP* (24Li)	5.65	1.17	0.103
<b><math>\text{Al}_{10}\text{N}_{10}+\text{Li}_4\text{O}</math></b>					
1.	BD (8N-19Al)	LP* (22Li)	16.8	1.51	0.142
2.	LP (18Al)	LP* (23Li)	54.23	0.77	0.206
3.	LP (18Al)	LP* (25Li)	31.73	0.99	0.184

intramolecular interactions. The variation of the charge of 19Al (–1.145 e) was observed in  $\text{Al}_{10}\text{N}_{10}+\text{Li}_4\text{N}$ . Unlike  $\text{Al}_{10}\text{N}_{10}+\text{Li}_4\text{N}$ , the Li atoms in the  $\text{Al}_{10}\text{N}_{10}+\text{Li}_4\text{O}$  have significantly varying stabilization energy.

However, the stabilization energy is higher for 23Li attached to an 18Al atom of nanocage. This was in good agreement with the optimized geometry of the  $\text{Al}_{10}\text{N}_{10}+\text{Li}_4\text{O}$  where the superalkali is attached through the bond 18Al – 23Li. Additionally, the 23Li atom impacts negatively to the total charge of the complex other than the rest of the Li atoms. Thus, the NBO and charge variation support the structural results of the superalkali-doped nanocage. The higher contribution of the superalkali was observed in the intramolecular interactions in the title nanocages and  $\text{Al}_{10}\text{N}_{10}+\text{Li}_4\text{N}$  is found to possess higher ICT compared to  $\text{Al}_{10}\text{N}_{10}+\text{Li}_4\text{O}$ .

### 3.6. Vibrational analysis

Raman spectra were simulated for the title nanocages to report the vibrational modes of the nanocages by performing polar calculations. The symmetric stretching ( $\nu$ ) of the N-Al bond of the  $\text{Al}_{10}\text{N}_{10}$  nanocage showed a peak at  $378.4\text{ cm}^{-1}$  and  $\nu_{\text{Al-Al}}$  at  $392.65\text{ cm}^{-1}$ . The asymmetric stretching ( $\alpha$ ) and torsional bending ( $\delta$ ) of the N-N bonds were observed towards the higher wavenumber. Modes with higher Raman intensity were observed for N-N and Al-Al bonds. A gradual increment in the vibrational peaks of the  $\text{Al}_{10}\text{N}_{10}$  nanocage was observed after the introduction of the superalkali. The major peaks were observed for the stretching of the bonds connecting the nanocage and superalkali (Fig. 5). The 21Li, 22Li, 23Li, and 24Li atoms bonded with the 19N in  $\text{Al}_{10}\text{N}_{10}+\text{Li}_4\text{N}$  structure gave higher Raman intensity modes at  $719\text{ cm}^{-1}$ . The  $\nu_{\text{Al-Al}}$  modes were observed at  $360.74\text{ cm}^{-1}$ . The other major

vibrational modes with higher Raman intensity are listed in SD 3. The peak at  $841.79\text{ cm}^{-1}$  in  $\text{Al}_{10}\text{N}_{10}+\text{Li}_4\text{O}$  showed the raised value of Raman intensity for  $\alpha_{22\text{Li-21O}}$  and  $\alpha_{25\text{Li-21O}}$ . Thus, the simulated Raman spectra showed enhancement in the vibrational peaks for the superalkali-adsorbed nanocage. However, the additional modes were significantly observed for Li, N, and O atoms of the superalkali. This observation is valid enough to state the active participation of the respective superalkali in the vibrational activities of the nanocages. The high Raman intensity was mainly obtained for the vibrational modes of inter-connecting bonds between the nanocage and superalkali. Moreover, the high value of Raman intensity leads to the high value of polarizability of the molecules [32]. Therefore, it is believed that the nanocages with high Raman intensity modes are a potential candidate for giving NLO responses.

### 3.7. Electronic transitions analysis

To investigate the nanocage's absorption maxima, TD-DFT computations were performed. Absorption spectra of pure  $\text{Al}_{10}\text{N}_{10}$ , superalkali doped  $\text{Al}_{10}\text{N}_{10}+\text{Li}_4\text{N}$ , and  $\text{Al}_{10}\text{N}_{10}+\text{Li}_4\text{O}$  have been plotted and shown in Fig. 6 and the transition details have been listed in SD 4. The absorption spectra of probe nanocage were observed between wavelength 300–600 nm with the crucial transition at 420 nm. This crucial transition with oscillator strength 0.0311 was responsible for the broad absorption band of the  $\text{Al}_{10}\text{N}_{10}$  nanocage. A prominent red shift was observed in the nanocage after the introduction of the superalkali. The  $\text{Al}_{10}\text{N}_{10}+\text{Li}_4\text{N}$  has a maximum absorption wavelength of 1030 nm and it also possesses a minimum band gap of 0.872 eV. The crucial transition for  $\text{Al}_{10}\text{N}_{10}+\text{Li}_4\text{O}$  was observed at wavelength 487 nm. However, the absorbance intensity of  $\text{Al}_{10}\text{N}_{10}+\text{Li}_4\text{O}$  was highly raised as compared to  $\text{Al}_{10}\text{N}_{10}+\text{Li}_4\text{N}$ . This might be due to the high electronegativity of the oxygen atom of  $\text{Li}_4\text{O}$ . The calculated absorption spectra for the title nanocages shows the maximum absorption wavelength corresponds to the electronic transition from HOMO to LUMO. Thus, the transitions are predicted as  $\pi-\pi^*$  transitions of  $\text{Al}_{10}\text{N}_{10}+\text{Li}_4\text{O}$  [33].

### 3.8. Applications as NLO materials

The literature has evidence that the introduction of the charge excessive systems to the organic compounds were found to be considered efficient in tuning the hyperpolarizabilities of the complex systems. The hyperpolarizabilities of the inorganic clusters were found to be high due to the availability of the excess diffused electrons [34]. The NLO

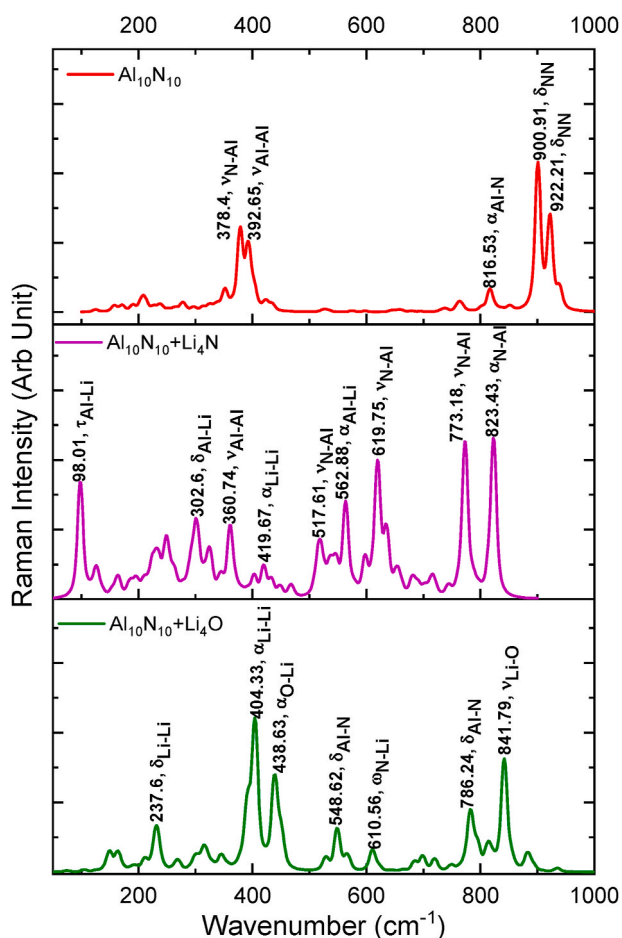


Fig. 5. Computed Raman spectra of (a)  $\text{Al}_{10}\text{N}_{10}$ , (b)  $\text{Al}_{10}\text{N}_{10}+\text{Li}_4\text{N}$ , and (c)  $\text{Al}_{10}\text{N}_{10}+\text{Li}_4\text{O}$  using UBVP86-6-311G(++,d,p) def2D2V set of functions (Symmetric stretching- $\nu$ , asymmetric stretching- $\alpha$ , torsional bending in plane (scissoring)- $\delta$ , twisting- $\tau$ , rocking- $\rho$ , and wagging- $\omega$ , bending of C – C bonds in benzene-  $\Theta$ , stretching of C – C bonds in benzene-  $\lambda$ ).

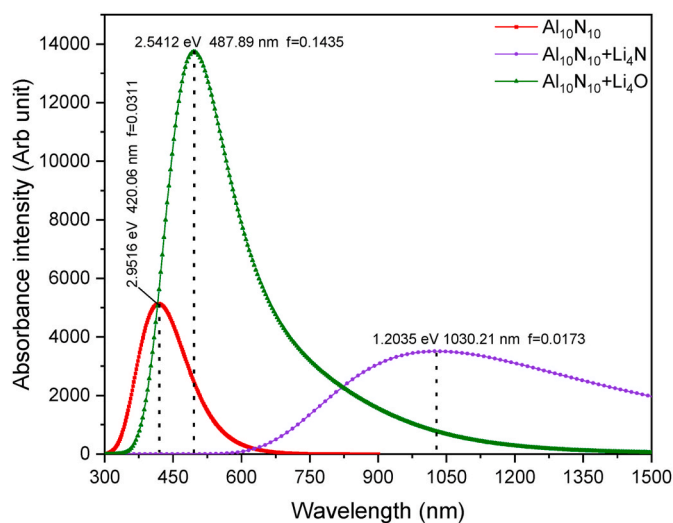


Fig. 6. Computed absorption spectra of (a)  $\text{Al}_{10}\text{N}_{10}$ , (b)  $\text{Al}_{10}\text{N}_{10}+\text{Li}_4\text{N}$ , and (c)  $\text{Al}_{10}\text{N}_{10}+\text{Li}_4\text{O}$ .

parameters for title complexes were computed using the polar calculations and the observed values were listed in Table 2. The value of  $\mu_{\text{total}}$  of probe  $\text{Al}_{10}\text{N}_{10}$  was computed as 1.538 Debye but the introduction of superalkali leads to increased values of  $\mu_{\text{total}}$  to 10.279 Debye for  $\text{Al}_{10}\text{N}_{10}+\text{Li}_4\text{N}$  and 14.932 Debye for  $\text{Al}_{10}\text{N}_{10}+\text{Li}_4\text{O}$ . The values of polarizability were also seen to be raised for the complexes. This reveals the enhanced linear optical activity in the superalkali adsorbed complexes. The value of  $\beta_{\text{total}}$  for the probe nanocage was reported as  $7.13 \times 10^{-30}$  esu. This value increases tremendously after the introduction of the nanocage. The values of  $\beta_{\text{total}}$  for  $\text{Al}_{10}\text{N}_{10}+\text{Li}_4\text{N}$  and  $\text{Al}_{10}\text{N}_{10}+\text{Li}_4\text{O}$  were evaluated as  $173.13 \times 10^{-30}$  esu and  $172.45 \times 10^{-30}$  esu respectively. The research had been previously done on the NLO responses of the  $\text{Al}_{12}\text{N}_{12}$  nanocage, but no such study was found in which the investigation for title nanocage was performed. Thus, the hyperpolarizability analysis determines the potent characteristics of  $\text{Al}_{10}\text{N}_{10}+\text{Li}_4\text{N}$ , and  $\text{Al}_{10}\text{N}_{10}+\text{Li}_4\text{O}$  clusters to be used as efficient NLO materials. In the literature, it was found that the alkali atoms were also engaged in the enhancement of the  $\beta_{\text{total}}$  of graphdiyne (GDY) making the combination efficient for NLO applications [35–38]. The  $\beta_{\text{total}}$  of different combinations like  $\text{Li}_3\text{NK@GDY}$  ( $2.88 \times 10^5$  a.u.),  $\text{Na}_3\text{S@GDY}$  ( $1.36 \times 10^5$  au),  $\text{Li@GY}$  ( $8.57 \times 10^4$  au),  $\text{K@GY}$  ( $3.93 \times 10^5$  a.u.), and  $\text{K}_3\text{O@GDY}$  ( $3.93 \times 10^5$  a.u.) were found to be higher after the introduction of the alkali atoms in the GDY systems. Therefore, the superalkali atoms are proved to be a best suited doping candidate for the enhancement of the NLO responses of pristine.

#### 4. Conclusion

The present study is the first-ever study done on the  $\text{Al}_{10}\text{N}_{10}$  nanocage with superalkalis ( $\text{Li}_4\text{N}$  and  $\text{Li}_4\text{O}$ ) as dopants. Designed  $\text{Al}_{10}\text{N}_{10}$ ,  $\text{Al}_{10}\text{N}_{10}+\text{Li}_4\text{N}$ , and  $\text{Al}_{10}\text{N}_{10}+\text{Li}_4\text{O}$  nanocages have been theoretically investigated through DFT. The research findings demonstrate that the designed nanocages have promising values of NLO parameters. The geometrical parameters showed the bonding between all the atoms of  $\text{Li}_4\text{N}$  with the nanocage, but in the case of  $\text{Li}_4\text{O}$ , there was partial bonding between one Li atom and the nanocage. Similar behavior was observed in MEP surfaces. Electron-donating and electron-withdrawing moieties were spotted in  $\text{Al}_{10}\text{N}_{10}+\text{Li}_4\text{N}$  but the MEP surface didn't spot any reactive sites in the  $\text{Al}_{10}\text{N}_{10}+\text{Li}_4\text{O}$  complex. Moreover, the DOS spectra reveal a significant decrement in the band gap of the nanocage after the introduction of superalkali. However,  $\text{Li}_4\text{N}$  behaves as the active donor but  $\text{Li}_3\text{O}$  doesn't reflect any reactivity. In  $\text{Al}_{10}\text{N}_{10}+\text{Li}_4\text{N}$ , the modes with higher Raman intensity were observed for all the Li atoms of the  $\text{Li}_4\text{N}$  superalkali, but a single Li atom attached to the nanocage in  $\text{Al}_{10}\text{N}_{10}+\text{Li}_4\text{O}$  gave a prominent peak in vibrational spectra. A similar kind of behavior was observed in electronic spectra also. The  $\text{Li}_4\text{O}$  adsorbed nanocage gave a high-intensity peak as compared to that of probe nanocage but the  $\text{Li}_4\text{N}$  adsorbed nanocage gave a significant shift in the wavelength of the spectral peak. This ensures the occurrence of  $\pi-\pi^*$  transitions that played a lead role in enhancing the polarizability of the molecules. The value of first-order hyperpolarizability was close enough for both the complex formed after the adsorption of superalkali but the reactivity descriptors and spectral analysis draw a potential candidature of  $\text{Al}_{10}\text{N}_{10}+\text{Li}_4\text{N}$  as NLO material. Therefore, the present study discovers  $\text{Li}_4\text{N}$  adsorbed  $\text{Al}_{10}\text{N}_{10}$  nanocage as the promising NLO structure that can be synthesized shortly and can be employed for several NLO applications.

#### Ethical approval

**Human and/or animal studies:**Not applicable.

**Consent to publication:** This material is the author's original work, which has not been previously published elsewhere. All authors have been personally and actively involved in substantial work leading to the paper and will take public responsibility for its content. The paper properly credits the meaningful contributions of all the co-authors.

**Table 2**

Computed NLO parameters for  $\text{Al}_{10}\text{N}_{10}$ ,  $\text{Al}_{10}\text{N}_{10}+\text{Li}_4\text{N}$ , and  $\text{Al}_{10}\text{N}_{10}+\text{Li}_4\text{O}$  nanocages.

Nanocage	$\mu_{\text{total}}$	$\alpha_{\text{total}}$	$\beta_{\text{total}}$
$\text{Al}_{10}\text{N}_{10}$	1.538	43.77	7.13
$\text{Al}_{10}\text{N}_{10}+\text{Li}_4\text{N}$	10.279	74.96	173.13
$\text{Al}_{10}\text{N}_{10}+\text{Li}_4\text{O}$	14.932	62.37	172.45

#### Availability of data and material

The sources of all the data and materials have been mentioned in the article.

#### Funding

S. Lakhera and M. Rana thank Uttarakhand Science Education and Research Centre (USERC), Department of Information and Science Technology, Government of Uttarakhand, for financial support through an R&D Research Project (Project no: USERC/2023-24/190).

#### CRediT authorship contribution statement

**Shradha Lakhera:** Writing – original draft, Visualization, Validation, Methodology, Investigation. **Meenakshi Rana:** Writing – review & editing, Supervision, Conceptualization. **Vivek Dhuliya:** Writing – original draft, Visualization, Resources.

#### Declaration of competing interest

The work: "Enhancement of the Electronic and Optical Properties of Super-alkali Metal Adsorbed  $\text{Al}_{10}\text{N}_{10}$  Nanocage" by Shradha Lakhera, Vivek Dhuliya, and myself is original research work done by the authors and have been submitted for publication in your esteemed journal "Materials Science in Semiconductor Processing" as an article.

#### Data availability

No data was used for the research described in the article.

#### Appendix A. Supplementary data

Supplementary data to this article can be found online at <https://doi.org/10.1016/j.mssp.2024.108882>.

#### References

- [1] W. Chen, Z.R. Li, D. Wu, Y. Li, C.C. Sun, F.L. Gu, Y. Aoki, Nonlinear optical properties of alkalides  $\text{Li}^+$  (calix [4] pyrrole)  $\text{M}(\text{M} = \text{Li}, \text{Na}, \text{and K})$ : alkali anion atomic number dependence, *J. Am. Chem. Soc.* 128 (2006) 1072–1073, <https://doi.org/10.1021/ja056314+>.
- [2] L.M. Abegao, R.D. Fonseca, F.A. Santos, G.B. Souza, A.L.B. Barreiros, M. L. Barreiros, M. Alencar, C.R. Mendonca, D.L. Silva, L. De Boni, Second- and third-order nonlinear optical properties of unsubstituted and mono-substituted chalcones, *Chem. Phys. Lett.* 648 (2016) 91–96.
- [3] S. Munsif, S. Khan, A. Ali, M.A. Gilani, J. Iqbal, R. Ludwig, K. Ayub, Remarkable nonlinear optical response of alkali metal doped aluminum phosphide and boron phosphide nanoclusters, *J. Mol. Liq.* 271 (2018) 51–64, <https://doi.org/10.1016/j.molliq.2018.08.121>.
- [4] M. Monajjemi, M. Khaleghian, EPR study of electronic structure of  $[\text{CoF}_6]^{3-}$  and  $\text{B}_18\text{N}_{18}$  nano ring field effects on octahedral complex, *J. Cluster Sci.* 22 (4) (2011) 673–692, <https://doi.org/10.1007/s10876-011-0414-2>.
- [5] S. Alvarez, J. Cirera, How high the spin? Allowed and forbidden spin states in transition-metal chemistry, *Angew. Chem. Int. Ed.* 45 (19) (2006) 3012–3020, <https://doi.org/10.1002/anie.200503492>.
- [6] Barazesh N. Shakerzadeh, S.J. Talebi, A comparative theoretical study on the structural, electronic and nonlinear optical features of  $\text{B}_{12}\text{N}_{12}$  and  $\text{Al}_{12}\text{N}_{12}$  nanoclusters with the groups III, IV and V dopants, *Superlattice. Microst.* 76 (2014) 264–276, <https://doi.org/10.1016/j.spmi.2014.09.037>.
- [7] W.M. Sun, D. Wu, Y. Li, Z.R. Li, Theoretical study on superalkali ( $\text{Li}_3$ ) in ammonia: novel alkalides with considerably large first hyperpolarizabilities, *Dalton Trans.* 43 (2014) 486–494, <https://doi.org/10.1039/c3dt51559a>.

- [8] S.B. Kolavekar, N. Ayachit, G. Jagannath, K. NagaKrishnakanth, S.V. Rao, Optical, structural and Near-IR NLO properties of gold nanoparticles doped sodium zinc borate glasses, *Opt. Mater.* 83 (2018) 34–42, <https://doi.org/10.1016/j.optmat.2018.05.083>.
- [9] I. Jeon, A. Shawky, H.S. Lin, S. Seo, H. Okada, J.W. Lee, A. Pal, S. Tan, A. Anisimov, E.I. Kauppinen, Controlled redox of lithium-ion endohedral fullerene for efficient and stable metal electrode-free perovskite solar cells, *J. Am. Chem. Soc.* 141 (2019) 16553–16558, <https://doi.org/10.1021/jacs.9b06418>.
- [10] S. Lakhera, M. Rana, K. Devlal, Influence of adsorption of gold and silver nanoclusters on structural, electronic, and nonlinear optical properties of pentacene-5, 12-dione: a DFT study, *Opt. Quant. Electron.* 55 (2023) 178, <https://doi.org/10.1007/s11082-022-04422-z>.
- [11] M. Rana, A. Chatterjee, P. Chowdhury, Investigation of nonlinear optical properties of organic based di amine substituted tetraphenylethylene, *AIP Conf. Proc.* 2009 (2018) 020055, <https://doi.org/10.1063/1.5052124>.
- [12] N. Kosar, T. Mahmood, K. Ayub, S. Tabassum, M. Arshad, M.A. Gilani, Doping superalkali on Zn12O12 nanocage constitutes a superior approach to fabricate stable and high-performance nonlinear optical materials, *Opt Laser. Technol.* 120 (2019) 105753, <https://doi.org/10.1016/j.optlastec.2019.105753>.
- [13] S. Muhammad, H. Xu, Y. Liao, Y. Kan, Z. Su, Quantum mechanical design and structure of the Li@B 10 H 14 basket with a remarkably enhanced electro-optical response, *J. Am. Chem. Soc.* 131 (2009) 11833–11840, <https://doi.org/10.1021/ja9032023>.
- [14] M.Y. Redko, J.E. Jackson, R.H. Huang, J.L. Dye, Design and synthesis of a thermally stable organic electride, *J. Am. Chem. Soc.* 127 (2005) 12416–12422, <https://doi.org/10.1021/ja053216f>.
- [15] M. Niu, G. Yu, G. Yang, W. Chen, X. Zhao, X. Huang, Doping the alkali atom: an effective strategy to improve the electronic and nonlinear optical properties of the inorganic Al 12 N 12 nanocage, *Inorg. Chem.* 53 (2014) 349–358, <https://doi.org/10.1021/ic4022917>.
- [16] Y. Arshad, M. Asghar, M. Yar, et al., Transition metal doped boron nitride nanocages as high performance nonlinear optical materials: a DFT study, *J. Inorg. Organomet. Polym.* (2023), <https://doi.org/10.1007/s10904-023-02546-7>.
- [17] F. Khaliq, T. Mahmood, K. Ayub, S. Tabassum, M.A. Gilani, Exploring Li4N and Li4O superalkalis as efficient dopants for the Al12N12 nanocage to design high performance nonlinear optical materials with high thermodynamic stability, *Polyhedron* 200 (2021) 15145, <https://doi.org/10.1016/j.poly.2021.115145>.
- [18] N. Kosar, T. Mahmood, K. Ayub, S. Tabassum, M. Arshad, M.A. Gilani, Doping superalkali on Zn12O12 nanocage constitutes a superior approach to fabricate stable and high-performance nonlinear optical materials, *Opt Laser. Technol.* 120 (2019) 105753, <https://doi.org/10.1016/j.optlastec.2019.105753>.
- [19] K. Ayub, Are phosphide nano-cages better than nitride nano-cages? A kinetic, thermodynamic and non-linear optical properties study of alkali metal encapsulated X 12 Y 12 nano-cages, *J. Mater. Chem. C* 4 (2016) 10919–10934, <https://doi.org/10.1039/C6TC04456E>.
- [20] A.S. Rad, K. Ayub, A comparative density functional theory study of guanine chemisorption on Al12N12, Al12P12, B12N12, and B12P12 nano-cages, *J. Alloys Compd.* 672 (2016) 161–169, <https://doi.org/10.1016/j.jallcom.2016.02.139>.
- [21] Chioma G. Apebende, Goodness J. Ogunwale, Hitler Louis, Innocent Benjamin, Michael T. Kadiri, Aniekian E. Owen, Amanda-Lee E. Manicum, Density functional theory (DFT) computation of pristine and metal-doped MC59 (M = Au, Hf, Hg, Ir) fullerenes as nitrosourea drug delivery systems, *Mater. Sci. Semicond. Process.* 158 (2023) 107362, <https://doi.org/10.1016/j.mssp.2023.107362>.
- [22] S. Lakhera, M. Rana, K. Devlal, I. Celik, R. Yadav, A comprehensive exploration of pharmacological properties, bioactivities and inhibitory potentiality of luteolin from *Tridax procumbens* as anticancer drug by in-silico approach, *Struct. Chem.* (2022), <https://doi.org/10.1007/s11224-022-01882-7>.
- [23] S. Lakhera, M. Rana, K. Devlal, V. Dhuliya, Quantum mechanical study of three aromatic bioactive fatty alcohol compounds with nonlinear optical and potential light harvesting properties, *Opt. Mater.* 129 (2021) 112476, <https://doi.org/10.1016/j.optmat.2022.112476>.
- [24] N.M. O'Boyle, A.L. Tenderholt, K.M. Langner, CcLib: a library for package-independent computational chemistry algorithms, *J. Comput. Chem.* 29 (2008) 839–845, <https://doi.org/10.1002/jcc.20823>.
- [25] M.J. Frisch, G.W. Trucks, H.B. Schlegel, G.E. Scuseria, M.A. Robb, J.R. Cheeseman, Gaussian, Inc., \*Gaussian 09\*, Gaussian, Inc., 2009.
- [26] R. Dennington, T.A. Keith, J.M. Millam, GaussView, SemicheM Inc. Shawnee Mission KS, 2019, Version 6.1.1.
- [27] R. Boyd, *Nonlinear Optics*, third ed., Elsevier, 2008. ISBN 978-81-312-2292-8.
- [28] S. Lakhera, M. Rana, K. Devlal, Comprehensive quantum chemical study of the associative complex of *para*-aminobenzoic acid and 7-diethylamino 4-methyl coumarin by adsorption and aromatic bridges, *J. Mol. Model.* 30 (2024) 37, <https://doi.org/10.1007/s00894-023-05816-w>.
- [29] S. Lakhera, M. Rana, K. Devlal, V. Dhuliya, Computational study of non-linear optical and electrical properties of 1,3-dinitropyrene, *Opt. Quant. Electron.* 55 (2023) 85, <https://doi.org/10.1007/s11082-022-04371-7>.
- [30] S. Lakhera, M. Rana, K. Devlal, Investigation of the electronic and optical activity of halogen-substituted 2-nitrotoluene by density functional theory, *Opt. Quant. Electron.* 55 (2023) 292, <https://doi.org/10.1007/s11082-023-04569-3>.
- [31] S. Lakhera, M. Rana, K. Devlal, N. Kanagathara, J. Janczak, Photovoltaic characteristics of organic heterocyclic 2,9-dimethyl quinacridone in different solvents using DFT approach, *J. Photochem. Photobiol., A* (2023) 114664, <https://doi.org/10.1016/j.jphotochem.2023.114664>.
- [32] M. Rana, P. Chowdhury, Effects of hydrogen bonding between pyrrole-2-carboxaldehyde and nearest polar and nonpolar environment, *Spectrochim. Acta A Mol. Biomol.* 185 (2017) 198–206, <https://doi.org/10.1016/j.saa.2017.05.050>.
- [33] M. Rana, N. Singla, A. Chatterjee, A. Shukla, P. Chowdhury, Investigation of nonlinear optical (NLO) properties by charge transfer contributions of amine functionalized tetraphenylethylene, *Opt. Mater.* 62 (2016) 80–89, <https://doi.org/10.1016/j.optmat.2016.09.043>.
- [34] M. Rana, N. Singla, A. Pathak, R. Dhanya, C. Narayana, P. Chowdhury, Vibrational-electronic properties of intra/inter molecular hydrogen bonded heterocyclic dimer: an experimental and theoretical study of pyrrole-2-carboxaldehyde, *Vib. Spectrosc.* 89 (2017) 16–25, <https://doi.org/10.1016/j.vibspec.2016.12.003>.
- [35] X. Li, Graphdiyne: A promising nonlinear optical material modulated by tetrahedral alkali-metal nitrides, *J. Mol. Liq.* 277 (2019) 641–645, <https://doi.org/10.1016/j.molliq.2018.12.128>.
- [36] N. Kosar, K. Shehzadi, K. Ayub, T. Mahmood, Theoretical study on novel superalkali doped graphdiyne complexes: unique approach for the enhancement of electronic and nonlinear optical response, *J. Mol. Graph. Model.* 97 (2020) 107573, <https://doi.org/10.1016/j.jmkgm.2020.107573>.
- [37] X. Li, S. Li, Investigations of electronic and nonlinear optical properties of single alkali metal adsorbed graphene, graphyne and graphdiyne systems by first-principles calculations, *J. Mater. Chem. C* 7 (2018) 1630–1640, <https://doi.org/10.1039/C8TC05392H>.
- [38] X. Li, Y. Zhang, J. Lu, Remarkably enhanced first hyperpolarizability and nonlinear refractive index of novel graphdiyne-based materials for promising optoelectronic applications: a first-principles study, *Appl. Surf. Sci.* 512 (2020) 145544, <https://doi.org/10.1016/j.apsusc.2020.145544>.